Navier–Stokes modeling of a Gaede pump stage in the viscous and transitional flow regimes using slip-flow boundary conditions

S. Giors[a)]
Varian S.p.A., I-10040 Leinì, Italy, and Dipartimento di Energetica, Politecnico, I-10129 Torino, Italy

F. Subba and R. Zanino
Dipartimento di Energetica, Politecnico, I-10129 Torino, Italy

(Received 29 September 2004; accepted 3 January 2005; published 1 March 2005)

A three-dimensional model for a Gaede pump, based on the Navier–Stokes equations with no-slip boundary conditions, was introduced by the authors in a previous work. A commercial computational fluid dynamics code was used to obtain the solution in an outlet pressure range corresponding to the viscous laminar regime and incipient transition to molecular flow and the validation against the experimental data showed a good level of accuracy in terms of compression ratio. However, the mechanical power dissipation predicted by the no-slip model shows a trend diverging from the measured data for decreasing pressure, in the transitional flow regime. As most of the mechanical power is dissipated into heat by viscosity, slip-flow boundary conditions are introduced here in order to model the transitional effects on the wall shear stress and improve the accuracy of the Navier–Stokes description at low pressure. The calculation is carried out up to Knudsen numbers $\mathrm{Kn} \approx 1$, showing a very good agreement of the Navier–Stokes model, even close to molecular flow conditions, and leaving a residual error acceptable for design purposes. The model is used to analyze the flow fields in the Gaede pump and explain its behavior. The slip model needs just one adjusting parameter, i.e., the momentum accommodation coefficient, but exhibits a small sensitivity to its variations. Hence it can predict the compression ratio and power dissipation of Gaede pumps of any size in their whole operating pressure range, from the laminar viscous regime down to the transition to the molecular flow regime. © *2005 American Vacuum Society.* [DOI: 10.1116/1.1865152]

I. INTRODUCTION

This paper is the prosecution of a previous work by the authors, dealing with the simulation of the compression test of a Gaede pump with a Navier–Stokes (NS) model, in viscous and incipient transitional flow regimes.[1] Now the analysis is extended to lower pressures and the dissipation of mechanical power is considered. The model is enriched with the introduction of slip-flow boundary conditions.

In a drag pump, most of the mechanical power required to keep the rotor spinning at the given operational speed is dissipated into heat owing to the friction between the rotor and the gas, due to the gas viscosity. The power to compress the gas is indeed negligible, because of the small pressure differences (e.g., 1–10 mbar) and mass flow rates (e.g., 10^{-6}–10^{-5} kg/s) involved in the typical applications of these devices. Friction dissipated power (W_f) and the resulting viscous heat generation have a direct impact on the rotor temperature, which is a critical design parameter. Hence, from the design point of view, the capability of a model to predict the dissipated mechanical power is as important as the capability to predict the compression performances.

The NS model introduced in our previous paper was solved using no-slip boundary conditions at the walls, commonly applied in high-pressure viscous flows. The comparison with the data showed a good level of agreement in the compression ratio (ratio of outlet to inlet pressure, at zero throughput: $K = p_{\mathrm{out}}/p_{\mathrm{in}}$), even when the model was used in a pressure range where the continuous hypothesis was no longer completely acceptable.

One question is whether or when the NS model can be efficiently applied to get useful and reliable results in vacuum pumps applications. The general answer is, of course, that it depends on the Knudsen number $\mathrm{Kn} = \lambda/d$, i.e., ratio of the mean free path λ to a characteristic length scale d of the flow. For a given pump, i.e., given d, Kn depends on the pressure p, because λ depends on p. According to the Chapman–Enskog theory,[2] the NS equations can be derived from the Boltzmann equation via a truncated perturbative solution, valid for $\mathrm{Kn} \ll 1$. Textbooks on rarefied gas dynamics,[3] state that the no-slip NS model can be applied for flows characterized by $\mathrm{Kn} \leqslant 10^{-2}$. With suitable modifications of the boundary conditions (slip-flow boundary conditions) the NS model can be further extended up to $\mathrm{Kn} \leqslant 10^{-1}$.[4]

In the present work we will show that the agreement of the no-slip NS model in terms of W_f is not good for $\mathrm{Kn} > 5 \cdot 10^{-2}$ and that slip-flow boundary conditions at the walls are necessary to reproduce correctly W_f. We will also try to understand the reasons of the different behavior of K and W_f, as regards the effect of slip-flow boundary conditions at low pressure.

The problem of modeling power dissipation in a Gaede pump was already faced by Cerruti *et al.*,[5] using the one-

a)Electronic mail: silvio.giors@varianinc.com

dimensional pumping leak theory from Helmer and Levi,[6] to calculate the pressure distribution, together with a transitional one-dimensional model for the shear stress at the walls. They showed that it is necessary to take into account the transition effects in the shear stress at the wall, in order to reproduce W_f. By introducing an effective viscosity, decreasing with increasing Knudsen number, they were able to reproduce the behavior of W_f in transition regime.Their model, however, failed at high pressure, in the developed viscous regime.

This work is organized as follows: in Sec. II the Gaede pump test is described, with particular emphasis on the measurement of the mechanical power. Section III shows the poor agreement of the no-slip NS model in terms of W_f, and introduces the slip-flow boundary conditions. The slip-flow NS model is described in Sec. IV. Section V shows the comparison of the slip-flow NS model results with the measured data and reports a discussion relevant for the design purpose. Finally, in Sec. VI, some conclusions and future work perspectives are summarized.

II. GAEDE PUMP TEST

An experimental Gaede pump was tested with nitrogen gas, to measure K and W_f. Its geometry is shown in Figs. 1 and 2, and the geometric dimensions and working parameters are listed in Table I. The rotor and the stator channels are machined by high precision turning and milling, from an aluminum alloy. Their surfaces are not atomically clean, but can be considered gas-contaminated surfaces (this feature will be relevant to model the gas surface interaction). A detailed description of the pump, of the measurement setup, and of the procedure to measure K can be found elsewhere,[1] and will not be repeated here. We describe in some detail the procedure to obtain W_f from the mechanical power W_{mech}, measured through a free deceleration test. The pump was first run up to the full speed for a given outlet pressure p_{out} (rotational speed $\omega_0 = 2\pi f \cong 4461$ rad/s, weakly dependent on p_{out}). Then the motor was switched off and the rotational speed ω logged at time steps t_i during the free deceleration transient at constant pressure. In Fig. 3 you can see the deceleration data $\omega_i = \omega(t_i)$, for the case $p_{\mathrm{out}} = 5$ mbar.

Knowing the polar moment of inertia of the rotor I_p, the torque is $T = I_p |d\omega/dt|$ and the mechanical power is given by $W_{\mathrm{mech}} = T\omega$. We were interested to calculate the power at the full speed ω_0: $W_{\mathrm{mech}} = I_p \omega_0 |d\omega/dt|_0$. A three-dimensional CAD model of the rotor was used to calculate the polar moment of inertia of the rotor, $I_p = 9.18 \cdot 10^{-4}$ Kg m^2. During the deceleration the rotational speed of the pump decreases and so the inlet pressure increases even if p_{out} is kept constant, owing to the fact that the compression is reducing. Nevertheless we were interested to measure the mechanical power at the full rotational speed, so only the first 5% of the deceleration transient $\omega(t_i)$ was used to calculate $|d\omega/dt|_0$, from the nominal speed to 95% of the nominal speed. In that small velocity range the pressure along the whole transient can be considered constant. The first 5% of the deceleration transient is approximately linear (see Fig. 3), and $|d\omega/dt|_0$ was calculated taking the slope of a linear least squares interpolation of the deceleration data: $|d\omega/dt|_0 = 18.248$ rad s^{-2} in the example of Fig. 3, referring to the case $p_{\mathrm{out}} = 5$ mbar.

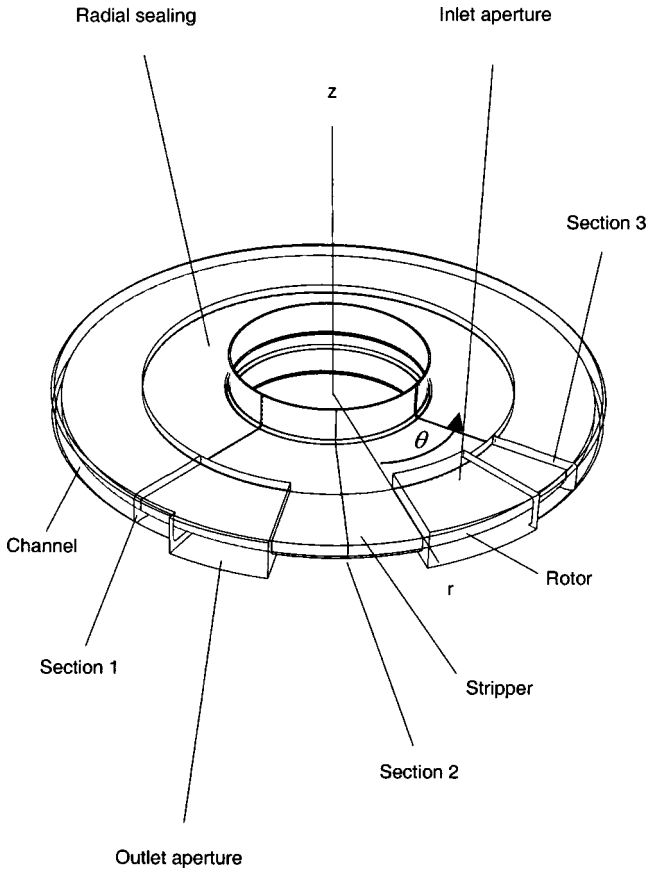

FIG. 1. Gaede pump 3D geometry. Sections 1,2,3 represent three cross sections passing for the rotation axis (z axis) and cutting the channel close to the outlet, the stripper and the channel close to the inlet, respectively. The sections 1 and 2 are detailed in Fig. 2. Section 3 has the same dimensions as section 1.

The mechanical power W_{mech}, measured as described above, includes the friction power W_f from the gas in the Gaede channel, in the sealing regions and in the motor chamber, and the power W_b dissipated by the bearings. The fric-

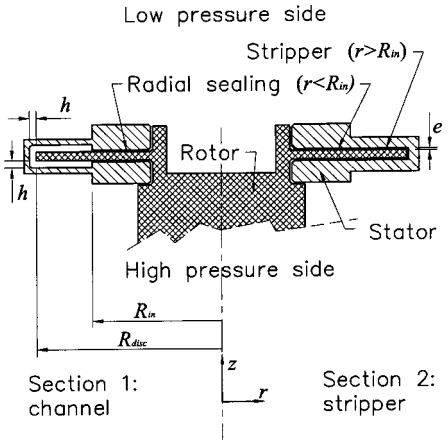

FIG. 2. Gaede pump cross sections.

TABLE I. Main geometrical dimensions and parameters of the tested Gaede stage. R_{disc} and R_{in} are the rotor radius and channel inner radius, respectively; h and e are the channel height (it is the same axial and radial) and the sealing gap height, respectively; $\Delta\theta_{ch}$, $\Delta\theta_{st}$, $\Delta\theta_{in}$, and $\Delta\theta_{out}$ are the angular extensions of the channel, stripper, inlet, and outlet apertures, respectively. f is the rotation frequency of the rotor.

R_{disc} (mm)	R_{in} (mm)	h (mm)	e (mm)	$\Delta\theta_{ch}$ (deg)	$\Delta\theta_{st}$ (deg)	$\Delta\theta_{in}$ (deg)	$\Delta\theta_{out}$ (deg)	f (Hz)
80	55.8	3.0	0.3	285	30	25	20	710

tion power dissipated in the motor chamber is negligible with respect to the power dissipated in the Gaede channel and sealing regions, because the motor radius is much smaller than the pump disc radius, so that both the surface area and the peripheral speed are much smaller. W_b does not depend on the pressure, and is measured when all the gas has been removed from the pump. It was measured through the deceleration test at a very low pressure (with outlet pressure $p_{out} < 10^{-3}$ mbar): Its value is about 10 W. It is a small correction at high pressure, but can be important at low pressure, hence it was subtracted from the total mechanical power measured at higher pressures in order to reproduce the W_f vs p_{out} characteristics: $W_f(p_{out}) = W_{mech}(p_{out}) - W_b$.

The precision of the indirect measurement of the mechanical power described above is estimated in $\pm 5\%$.

The described experiment was carried out in a wide pressure range, 0.1 mbar $< p_{out} <$ 25 mbar. If we consider the ratio of the maximum outlet pressure (i.e., 25 mbar) to the minimum inlet pressure (i.e., $2.5 \cdot 10^{-2}$ mbar), the whole pressure range present in the pump covers about three decades, in which the flow regime changes as well. The flow regime can be defined introducing some nondimensional parameters: Knudsen number, Kn, Reynolds number, Re, and Mach number, M.

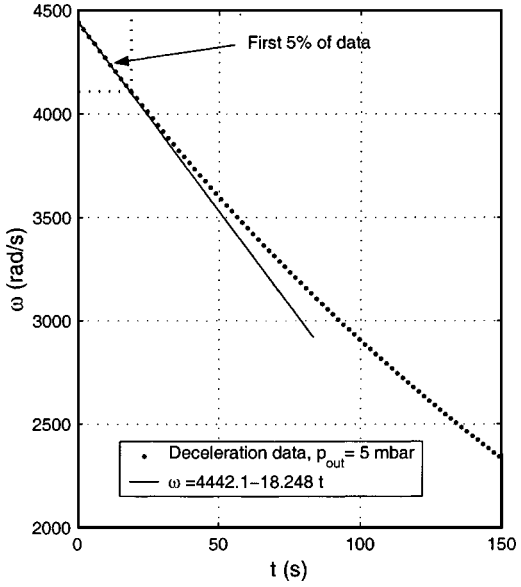

FIG. 3. Angular velocity data from the deceleration transient at $p_{out} = 5$ mbar: Extended transient (dotted) and least-squares linear interpolation of the first 5% of the transient (solid).

Kn was arbitrarily defined as the ratio of the nitrogen mean free path at the inlet pressure (where it assumes the maximum value in the pump), and the height h of the channel: $\mathrm{Kn} = \lambda(p_{in})/h$, where $\lambda(p_{in}) = \mu v_m / p_{in}$, μ is the viscosity and $v_m = \sqrt{2k_BT/m}$ is the most probable velocity of the gas molecules, with mass m and temperature T; k_B is the Boltzmann constant. This choice was motivated by the fact that the channel is the part of the domain that mostly contributes to the performances of the pump. Other choices are possible for the characteristic dimension, in particular we could base Kn on the gap e. We must be aware of the fact that, for a given pressure distribution, Kn calculated in the gap can be up to 10 times higher than Kn in the channel.

Re can be based on the density corresponding to the outlet pressure through the ideal gas law, $\rho_{out} = m p_{out}/k_BT$, the disc's maximum speed $V = 2\pi f R_{disc}$ and the height of the channel: $\mathrm{Re}_h = \rho_{out} V h/\mu$. This definition is arbitrary, but was chosen as being representative of the inertial-to-viscous-forces ratio in the channel. Other definitions are possible, specifically one used for Couette flow in shrouded rotor-stator systems (flow between a smooth rotor and a casing), where $\mathrm{Re}_\phi = \rho_{out}\omega R_{disc}^2/\mu$ is generally used.[7,8]

The Mach number was defined as the ratio of the disc's maximum speed $V = 2\pi f R_{disc}$, to the nitrogen speed of sound at 300 K temperature.

In the considered pressure range, 0.1 mbar $< p_{out} <$ 25 mbar, we have $1 > \mathrm{Kn} > 10^{-3}$, $7 < \mathrm{Re}_h < 1800$, $1.7 \cdot 10^2 < \mathrm{Re}_\phi < 4.4 \cdot 10^4$ and $\mathrm{M} \cong 1$ (owing to the constant speed of the rotor).

Re_h was defined thinking to the Gaede pump as a plane channel. The comparison with the standard Poiseuille flow in a pipe suggests that we are in a viscous laminar regime ($\mathrm{Re}_h < 2000$), but the Gaede pump fluid dynamics is more complicated, because of the presence of Couette drag flow superimposed to Poiseuille flow, the sharp bend of the streamlines approaching the stripper and the circular geometry.

Daily and Nece,[7] studied the Couette flow in shrouded rotor-stator systems, identifying two laminar regimes, for $\mathrm{Re}_\phi < 10^5$ and two turbulent regimes above. The two laminar regimes are characterized the first by merged boundary layer, dominated by diffusion effects ($\mathrm{Re}_\phi < 10^3$), the second by separated boundary layers, dominated by convection and centrifugal forces ($5 \cdot 10^3 < \mathrm{Re}_\phi < 10^5$). The two turbulent regimes are also characterized by merged and separate boundary layers. These works seem to confirm that we are in viscous laminar regime.

Since, to the best of our knowledge, there are no experimental data available in the literature on the laminar stability of our specific experimental situation, in this work we will use a viscous laminar NS model.

The Mach number close to 1 suggests that compressibility effects have to be included in the model.

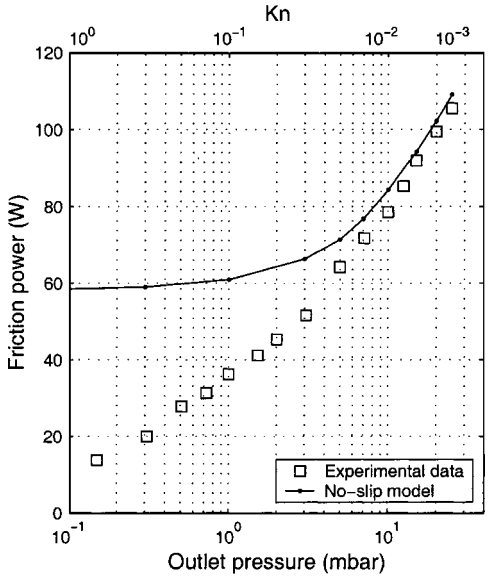

FIG. 4. No-slip model friction power compared with the experimental data, for varying outlet pressure.

III. NO-SLIP MODEL RESULTS AND NEED FOR SLIP-FLOW BOUNDARY CONDITIONS

In a previous paper we described a no-slip NS model for the Gaede pump, and compared the results with the experimental data in terms of zero throughput pumping performances (K or pressure difference Δp).[1]

The agreement was pretty good, up to $\mathrm{Kn} \approx 10^{-1}$. Even if we were using a model inconsistent with the expected flow regime, we found an acceptably good agreement of the no-slip model with the data in terms of K, in the considered pressure range.

Here we compare the no-slip model results with the data in terms of W_f (see Fig. 4): The agreement is good at high pressure, where the viscous flow hypotheses is fulfilled, but is getting worse at lower pressures, when $Kn \geqslant 5 \cdot 10^{-1}$.

In order to extend the accuracy of the NS model, even in terms of W_f, up to $Kn \leqslant 1$, the introduction of different boundary conditions at the wall is now considered.

General formulation of the slip-flow boundary conditions

The slip-flow boundary conditions are a mean to take into account the rarefaction effects in the framework of the NS formulation of gas dynamics, in the case of not extremely rarefied (i.e., not too large Kn) conditions. They include viscous and thermal slip (for tangential momentum equation) and thermal jump (for energy equation) boundary conditions.

The interaction of the molecules with a wall happens in a layer adjacent to the wall, about one mean free path thick, called the Knudsen layer. In this layer the gas molecules collide both among themselves and with the wall, transferring momentum and energy at each collision.

The velocity slip and thermal jump boundary conditions are used to model what happens in this layer, stating that there is a difference between the macroscopic tangential component of the gas velocity $u_{\tau,\mathrm{gas}}$ close to the wall and the wall velocity $u_{\tau,\mathrm{wall}}$ (velocity slip), as well as between the gas temperature T_{gas} close to the wall and the wall temperature T_{wall} (temperature jump). These differences are related to the normal ($\partial/\partial n$) and tangential ($\partial/\partial \tau$) gradients of the bulk gas velocity and temperature. The general form of the slip-flow boundary conditions reads:[9]

$$u_{\tau,\mathrm{gas}} - u_{\tau,\mathrm{wall}} = \sigma_P \lambda \frac{\partial u_{\tau,\mathrm{gas}}}{\partial n} + \sigma_T \frac{\mu}{\rho} \frac{\partial \ln(T_{\mathrm{gas}})}{\partial \tau}, \tag{1a}$$

$$T_{\mathrm{gas}} - T_{\mathrm{wall}} = \varsigma_T \lambda \frac{\partial T_{\mathrm{gas}}}{\partial n}, \tag{1b}$$

where $\lambda = \mu v_m / p$, μ is the gas viscosity, p is the local pressure, T is the local temperature, $\rho = pm/k_B T$ is the density and $v_m = \sqrt{2k_B T/m}$ is the most probable velocity of the gas molecules, with mass m (k_B is the Boltzmann constant). The coefficients σ_P, σ_T, ς_T are called viscous slip, thermal slip (or thermal creep) and thermal jump coefficients, respectively, and are dimensionless quantities $O(1)$.

The slip-flow boundary conditions model a resistance to the momentum and energy flux from the continuous gas bulk to the surface, localized in the Knudsen layer. This resistance is proportional to the mean free path, and becomes negligible when the mean free path is much smaller than the characteristic length scale of the flow, i.e., $\mathrm{Kn} \ll 1$. In fact the slip conditions reduce to the no-slip ones for negligible Kn. The NS equations with slip-flow boundary conditions can be rigorously derived form the Boltzmann equations, and they can be applied up to Knudsen numbers $\mathrm{Kn} < 0.1$.[4] For even higher Knudsen numbers local thermal equilibrium is no longer present, because the mean free path becomes comparable with the dimensions of the system, and the NS equations are no longer consistent with the physics of the problem. The parameters σ_P, σ_T, and ς_T in Eq. (1) are macroscopic coefficients which take into account the interaction of the gas molecules with the solid surface, and depend, in general, on the particular gas–solid couple. They can be expressed in terms of microscopic quantities called accommodation coefficients. An accommodation coefficient $\varepsilon(\varphi)$ can be defined for any molecular property $\varphi(\mathbf{v})$ (like momentum or energy) and represents an integral characteristics of the molecular distribution function $f(\mathbf{v})$ at the wall[12]

$$\varepsilon(\varphi) = \frac{\int_{v_n<0} \varphi(\mathbf{v}) |v_n| f(\mathbf{v}) d\mathbf{v} - \int_{v_n>0} \varphi(\mathbf{v}) |v_n| f(\mathbf{v}) d\mathbf{v}}{\int_{v_n<0} \varphi(\mathbf{v}) |v_n| f(\mathbf{v}) d\mathbf{v} - \int_{v_n>0} \varphi(\mathbf{v}) |v_n| f_w^{MB}(\mathbf{v}) d\mathbf{v}}, \tag{2}$$

where v_n is the normal component of the velocity, and f_w^{MB} is the Maxwell–Boltzmann distribution function with the surface temperature and the number density providing the molecular flux of the reflected particles equal to the incident one. For instance, if $\varphi(\mathbf{v}) = m v_\tau$ (v_τ is the tangential component of molecular velocity) we get the accommodation coef-

ficient for tangential momentum $\alpha_t=\varepsilon(mv_\tau)$. If $\varphi(\mathbf{v})=mv_n^2/2$ we get the accommodation coefficient for kinetic energy associated with the normal motion $\alpha_n=\varepsilon(mv_n^2/2)$. The quantity $[1-\varepsilon(\varphi)]$ represents the part of the information about a specific property $\varphi(\mathbf{v})$ that an average incident molecule keeps after a collision with the wall.

Accommodation coefficients refer to the interaction of the gas molecules with the surface and hence do not depend on the flow regime. As a consequence they can be measured in molecular flow conditions, where analytical expressions exist relating accommodation coefficients to some macroscopic measurable quantities (e.g., pressure drop through capillaries, or heat exchange from a heated wire).

The mathematical relation between slip and jump coefficients and accommodation coefficients is based on the solution of the Boltzmann equation in the Knudsen layer, assuming a particular model for collision integral and for the gas–surface interaction at the wall.

One of the first theoretical estimations of the slip and jump coefficients was done by Maxwell in 1879,[10] in terms of a single accommodation coefficient α, whose significance is that a fraction $(1-\alpha)$ of the molecules undergoes a specular reflection, while the remaining α is diffused with the Maxwellian distribution of the wall:

$$\sigma_P=\frac{\sqrt{\pi}}{2}\frac{2-\alpha}{\alpha}=0.886\frac{2-\alpha}{\alpha};\quad \sigma_T=0.75;\qquad \varsigma_T=\frac{15\sqrt{\pi}}{16}=1.662. \tag{3}$$

A more recent result is from Sharipov,[9] who solved a Boltzmann model equation in the Knudsen layer, using the Cercignani–Lampis scattering kernel at the wall.[11] This kernel models the gas–surface interaction introducing two accommodation coefficients, one for the tangential momentum, α_t, and one for the part of the kinetic energy associated with the normal motion α_n. Sharipov presented a table of numerical results and also the following interpolation formulas valid for the case $\alpha_n=1$ (perfect accommodation of kinetic energy, typical of the interaction of heavy gases, like nitrogen, with commercial metal surfaces, like aluminum):

$$\sigma_P=1.018\frac{2-\alpha_t}{\alpha_t}-0.264\frac{1-\alpha_t}{\alpha_t};\ \sigma_T=1.175;\ \varsigma_T=1.954. \tag{4}$$

In the following section we will describe the particular formulation of slip and jump boundary conditions and coefficients used in this work.

Looking for experimental results about the values of the accommodation coefficients as reported in the available literature, we found that the momentum accommodation coefficient does not depend much on the surface material as far as the surface is rough, or it is smooth but contaminated, i.e., not atomically clean[12] (because in this last case a contaminating atmospheric gas layer is adsorbed by the surface). As already stated, here we are interested in the interaction of nitrogen gas with contaminated aluminum surfaces. We did not find the data for such an exact situation, but we found some dispersed data for momentum accommodation coefficients in the range (0.8, 1) in similar situations (nitrogen gas interacting with contaminated surfaces of different materials). As far as the energy accommodation coefficient is concerned, we found that it differs significantly from unity only for light gases, and we found data in the range (0.8, 0.9) for nitrogen on glass, copper, and platinum surfaces.[13]

Hence, in this work, we will take, as a reference, the value $\alpha_t=\alpha_n=0.91$, reasonably acceptable for the nitrogen–aluminum couple, and we will carry out a parametric analysis to verify the sensitivity of K and W_f to the value of both accommodation coefficients in the range (0.8, 1).

TABLE II. Nitrogen gas properties temperature dependence: viscosity follows Sutherland's law, $\mu=\mu_0(T/T_0)^{3/2}(T_0+S)/(T+S)$; thermal conductivity follows a polynomial law, $k(T)=A_1+A_2T+A_3T^2$.

M	28.0134 kg/kmol		
	μ_0	T_0	S
μ	$1.663\ 10^{-5}$ Pa s	273.11 K	106.67 K
	A_1	A_2	A_3
k	$4.737\ 10^{-3}$ W/m/K	$7.272\ 10^{-5}$ W/m/K^2	$-1.122\ 10^{-8}$ W/m/K^3

IV. THE SLIP-FLOW MODEL: EQUATIONS AND BOUNDARY CONDITIONS

According to the discussion about the value of Kn, Re, and Ma introduced in Sec. II, the slip-flow model is based on the compressible NS equation, for a laminar flow. The energy equation and the viscous heating are included. The ideal gas law is used as equation of state: $p=\rho R^*T$, where $R^*=R/M$, $R=8.3145$ J K^{-1} mol^{-1}, $M=28.0134$ kg/kmol. Even if the gas temperature variations are not large compared to the absolute average temperature (about 10%), we enabled the gas transport properties to vary with temperature, because this improved the model's accuracy without increasing its computational cost. We used Sutherland's law for viscosity and a polynomial law for thermal conductivity (see Table II).

As far as the slip-flow boundary conditions are concerned, we simplified their general formulation [Eq. (1)], observing that the thermal creep term is negligible in our particular problem. In fact

$$\frac{\sigma_T\frac{\mu}{\rho}\frac{d\ln(T)}{d\tau}}{\sigma_P\frac{\mu v_m}{p}\frac{du_\tau}{dn}}\approx\frac{\sigma_T}{\sigma_P}\frac{\Delta T_{\text{gas}}}{T_{\text{gas}}}\frac{h}{L_{\text{ch}}}\frac{v_m}{V_{\text{rotor}}}\approx 1\cdot 10^{-1}\cdot 10^{-2}\cdot 1\approx 10^{-3}, \tag{5}$$

because the temperature variations are about 10% of the average absolute temperature, and the length of the channel L_{ch} is about 100 times greater than its height h.

Since the solution of the problem was carried out with the commercial CFD solver FLUENT,[14] we decided to use its

built-in formulation for viscous slip and thermal jump equations and coefficients:

$$u_{\tau,\mathrm{gas}} - u_{\tau,\mathrm{wall}} = \sigma_P \lambda \frac{\partial u_{\tau,\mathrm{gas}}}{\partial n}, \tag{6a}$$

$$T_{\mathrm{gas}} - T_{\mathrm{wall}} = \varsigma_T \lambda \frac{\partial T_{\mathrm{gas}}}{\partial n}, \tag{6b}$$

with

$$\sigma_P = \frac{2-\alpha_t}{\alpha_t}; \quad \varsigma_T = 2\frac{2-\alpha_n}{\alpha_n} \tag{7}$$

which are quite similar to Sharipov's formulation [Eq. (4)] when, as occurs in our problem, the accommodation coefficients are close to 1. Also the expression used for λ in Eq. (6) is different from the one used in Eq. (1) (based on viscosity). It is based on the Lennard-Jones characteristic length for nitrogen $\delta = 3.621$ Å : $\lambda = k_B T/\sqrt{2}\pi\delta^2 p$, where T and p are the gas local temperature and pressure, k_B is the Boltzmann constant.

Two types of boundaries are present in the numerical formulation of the problem: walls and outflow (there are no inlet boundaries because we are interested to simulate a compression test, with zero mass flow rate). On the walls viscous slip (for the momentum equation) and thermal jump (for the energy equation) boundary conditions were used. The measured velocity and temperature of rotor and stator walls were applied as boundary conditions. On the outflow boundary the static pressure is prescribed, while vanishing normal gradient is set for all the other scalars. From the same simulation we could calculate, in a post-processing phase, both K and W_f.

V. SLIP-FLOW MODEL RESULTS AND DISCUSSION

The model was solved using the commercial Finite Volume CFD solver Fluent.[14] The computational domain included a portion of the inlet chamber (attached to inlet aperture) and outlet chamber (attached to outlet aperture), in order to allow the self-consistent calculation of the radial leaks from and to those chambers. The computational grid used to obtain the results presented in this paper was made of about 300 000 hexahedral cells and a detail is shown in Fig. 5. It is a nonuniform, block structured, boundary fitted grid, well aligned with the cylindrical (r, ϑ, z) coordinates and also with the main flow directions in the channel (the higher gas velocity component is u_ϑ), and refined close to the walls. The solution was carried out using first-order and second-order upwind discretization schemes. The first-order was chosen after verifying that the differences on K and W_f with respect to the second-order scheme were less than 1%. The segregated solver (SIMPLE algorithm) was used to linearize the system of NS equations. The numerical accuracy of the results was checked monitoring the convergence of selected macroscopic quantities (K and W_f) during the solver iterations and repeating the calculation on a second systematically refined grid, with about 800 000 cells. The estimated numerical error for both K and W_f was $\leqslant 2\%$.

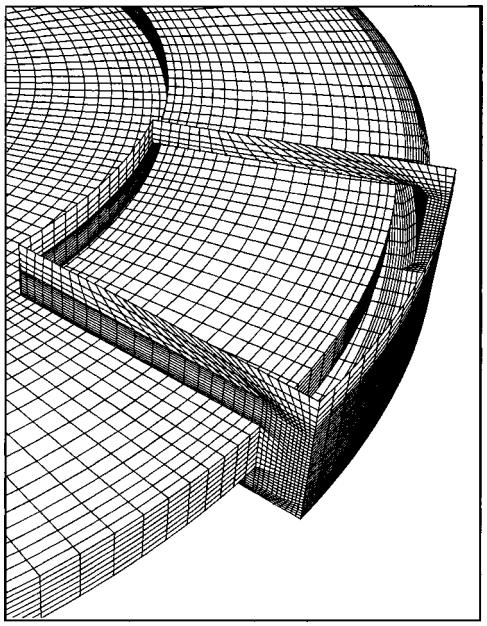

FIG. 5. Detail of the surface computational mesh close to the inlet aperture.

We failed attempting to reach a stationary laminar solutions for $p_{\mathrm{out}} > 10$ mbar, where some oscillations were detected. The oscillations were detected on both K and W_f, but their amplitude was very small (less than 2%). The nature of these oscillations was not numerical, because they persisted even on the finer grid. We accepted those solutions taking an average value of the oscillating inlet pressure and power. The comparison with the data will show that we are not committing a big error. The issue of laminar stability of the flow at high pressures will be discussed later.

A. Results of the reference case

We chose the case $p_{\mathrm{out}} = 1$ mbar, corresponding to Kn $\approx 10^{-1}$, as a reference case for the slip-flow model. We solved it with the following choice of the accommodation coefficients, for nitrogen gas and aluminum walls: $\alpha_t = \alpha_n = 0.91$. Some pictures of the flow fields for this case are reported in Figs. 6 and 7.

In Fig. 6 the contours of constant pressure are drawn on the surface of the rotor disc. The compression occurs almost entirely in the last quarter of the channel, close to the outlet, while the first three-quarters of the channel keep a uniform pressure. This result is in qualitative agreement with the predictions of the one-dimensional model from Helmer and Levi.[6] It is a characteristic behavior of the Gaede pump, when $p_{\mathrm{out}} \ll \Delta p_0$, where $\Delta p_0 = 6\mu V L_{\mathrm{ch}}/h^2$, is the maximum pressure difference that the pump with disc velocity V, channel length L_{ch} and channel height h, can give according to the one-dimensional model. The compression effect occurring in the stripper ($p_{\max} = 1.66$ mbar $> p_{\mathrm{out}}$) confirms the results obtained with a previous no-slip model.[1]

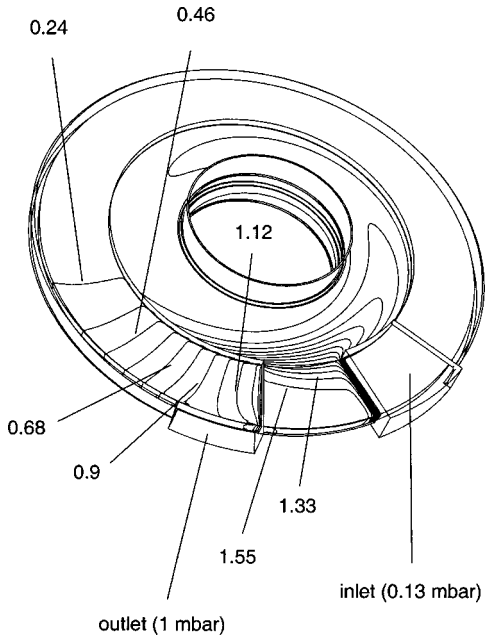

FIG. 6. Results of the reference case, $p_{out}=1$ mbar, $\alpha_t=\alpha_n=0.91$. Contours of constant absolute pressure on the rotor disc surface (mbar). The distance between adjacent contours is 0.11 mbar. The distance between labeled contours is 0.22 mbar.

In Fig. 7 the axial profiles of the tangential component $u_\theta(z)$ of the gas velocity are drawn at $r=R_{disc}$, for two angular positions, one close to the outlet (section 1), and the other close to the intlet (section 3). It is interesting to note that the tangential velocity close to the outlet exhibits negative values close to the stator walls (Poiseuille backflow), while the profile is close to linear at the inlet (Couette). This back-flow is due to the tangential pressure gradient and it is going to disappear at the inlet, where the pressure is uniform. The three-dimensional model confirms the typical Couette–Poiseuille velocity profile, shown by the one-dimensional models.[6] It is worthwhile to note the effect of the boundary conditions, which allows the gas to slip along the walls (e.g., the gas velocity close to the rotor is about 300 m/s, while the rotor surface is moving at about 355 m/s).

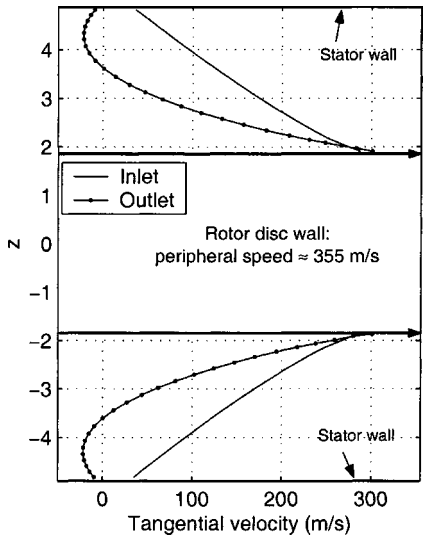

FIG. 7. Results of the reference case, $p_{out}=1$ mbar, $\alpha_t=\alpha_n=0.91$. Profiles of the tangential velocity component, $u_\vartheta(r=R_{disc}, z, \theta=const)$, on section 1 (outlet) and section 3 (inlet).

TABLE III. Sensitivity of K and W_f at $p_{out}=1$ mbar, to the accommodation coefficients. $\Delta K/K_0$ and $\Delta W_f/W_{f0}$ are the (percentage) differences, relative to the reference case, obtained with $\alpha_t=\alpha_n=0.91$: $K_0=6.188$, $W_{f0}=35.86$ W.

α_n	α_t	σ_P	ζ_T	K	$\Delta K/K_0$ (%)	W_f (W)	$\Delta W_f/W_{f0}$ (%)
0.91	0.8	1.5	2.395	6.153	−0.56	32.89	−8.2
0.91	1.0	1.0	2.395	6.211	0.37	38.04	6.1
0.8	0.91	1.198	3.0	6.192	0.06	35.91	0.1
1.0	0.91	1.198	2.0	6.184	−0.06	35.83	−0.08

The numerical macroscopic results, for K and W_f, are reported in Table III for the reference case. A sensitivity analysis was also performed, motivated by our uncertainty on the slip-flow coefficients, to check the effects of the accommodation coefficients on those results. The details on the sensitivity analysis are reported in Appendix A. The conclusion of that analysis is that the effects of variation of α_n on both K and W_f are negligible. The effect of α_t is remarkable on W_f only: $\Delta\alpha_t/\alpha_t\approx-10\%$ with respect to the reference value produces $\Delta W_f/W_{f0}\approx-8\%$; $\Delta\alpha_t/\alpha_t\approx+10\%$ with respect to the reference value produces $\Delta W_f/W_{f0}\approx+6\%$.

B. Experimental validation

The model was used to calculate K and W_f for different outlet pressures, from 10^{-1} to 25 mbar. The comparison of the model results with the experimental data is reported in Fig. 8(a) for K and Fig. 8(b) for W_f. Both slip-flow and no-slip model results are reported for comparison. Slip-flow results are reported for three values of the tangential momentum accommodation coefficients: 0.8, 0.91, and 1. The outlet pressure range in which we extended the calculation covers about three decades of pressure and Kn, if we consider the maximum outlet pressure (25 mbar) and the minimum inlet pressure (about $2.5\cdot10^{-2}$ mbar). In this pressure range the flow regime changes from viscous to molecular.

The agreement of K is good in the whole pressure range. The differences between no-slip and slip-flow model are small, but the slip-flow model results are closer to the experimental data. There is no significant effect of the accommodation coefficient at any pressure, as already stated for the reference case. The residual disagreement between slip-flow models and the data at low pressure ($p_{out}<1$ mbar, $\mathrm{Kn}>10^{-1}$) is about 10%.

The agreement between the slip-flow model and the measured W_f is very good in the whole pressure range. The slip-flow model reproduces very well the trend of the W_f vs outlet pressure curve. The differences between no-slip and slip-model are remarkable below 5 mbar ($\mathrm{Kn}>5\cdot10^{-2}$). There is some significant effect of the tangential accommodation co-

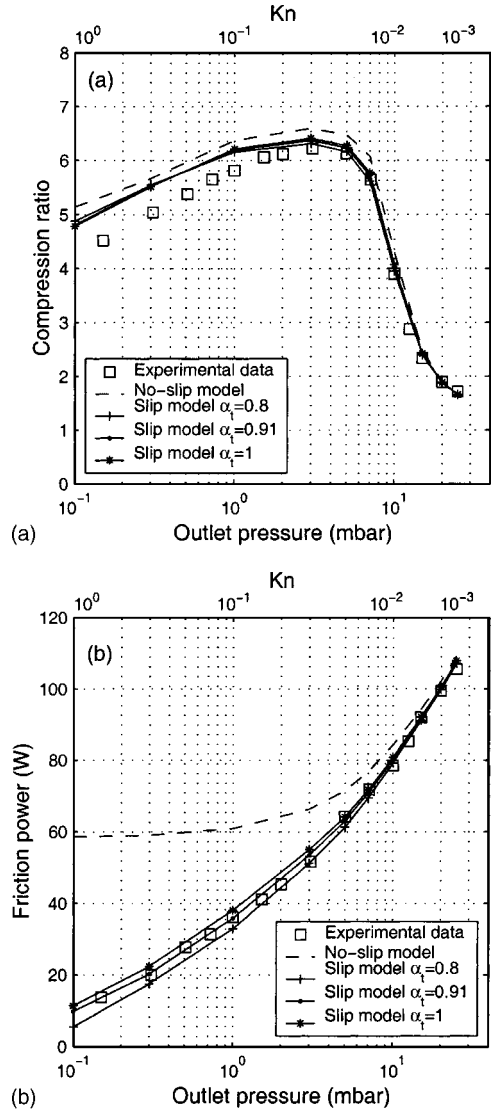

FIG. 8. Slip-flow model compared with no-slip model and experimental data: (a) compression ratio vs outlet pressure; (b) friction power vs outlet pressure.

efficient at lower pressures, as already stated for the 1 mbar case. The residual error between the reference slip model ($\alpha_t=\alpha_n=0.91$) and the data, in the whole pressure range, is about 3% or less.

C. Discussion

At high pressure ($p_{\text{out}}>10$ mbar, $\text{Kn}<0.01$) the slip model results match the no-slip results (see Fig. 8), both in terms of K and of W_f. This is in agreement with the mathematical form of the slip-flow boundary conditions at the walls [Eq. (1)], which reduce to the no-slip boundary conditions for small Kn.

The effect of the introduction of viscous slip and thermal jump boundary conditions on K at low pressure is very small. This is due to a particular feature of any properly designed Gaede pump, in which the leak through the radial sealing (the leak through the radial sealing is the algebraic sum of the leak from the high pressure outlet chamber into the channel and the one from the channel into the low pressure inlet chamber), is small with respect to the "pumping leak" through the stripper (the "pumping leak" is the one directly dragged by the disk motion through the stripper from the outlet into the inlet of the Gaede channel). As a consequence the limiting factor of K is the pumping leak throughput crossing the stripper.[6] This pumping leak, for a well designed stripper (not too short in tangential direction, otherwise the pressure difference across the stripper gives an extra nonnegligible Poiseuille contribution to the leakage), is of Couette flow type. One-dimensional solution of Couette flow between a stationary and a moving plate, with slip boundary conditions, shows that Couette flow's throughput is not affected by slip boundary conditions. In fact, in spite of the variation of the velocity profile, the average speed is kept equal to half the velocity of the plate at any Knudsen number (see Appendix B). There is no reason why this behavior should be different in our three-dimensional model, because the flow in the stripper is close to one-dimensional, thanks to the very small gap-to-angular length ratio.

Slip-flow computed W_f vanishes at very low pressure, where the gas is getting extremely rarefied, as shown by the data. W_f is given by the friction torque times the angular rotational speed ω: $W=T\cdot\omega$. The friction torque is the integral of the ϑ component of the shear stress acting on the wall, $\tau_{\text{wall},\vartheta}$, times the radius r, on the surface of the rotor:

$$T=\oint\!\!\!\oint_{\text{Rotor surface}} |\tau_{\text{wall},\vartheta}| r dA. \tag{8}$$

Most of the rotor surface has a normal pointing in the z direction, so that $\tau_{\text{wall},\vartheta}=\mu\,(\partial u_\vartheta/\partial z)|_{\text{wall}}$. A similar expression can be written for the cylindrical surfaces, involving the velocity derivative $\partial u_\vartheta/\partial r$.

The no-slip model does not reproduce the dramatic reduction of W_f occurring in the transition to molecular flow, but rather seems to reach an asymptotic value (about 60 W) at low pressure. Actually the no-slip model cannot reproduce this effect reducing the pressure because the no-slip boundary conditions at the walls correspond to a nonvanishing asymptotic value for the velocity gradient, and the gas viscosity is a constant. The slip-flow model, on the other hand, is able to reproduce the decrease of power with pressure, showing a very good agreement with the data, thanks to the fact that the velocity gradient is a decreasing function of Kn. This is shown, for example, by the solution of the one-dimensional Couette model with viscous slip boundary conditions (see Appendix B), and can also be shown qualitatively by the analytic form of the boundary condition [Eq. (6a)]: If $\lambda\to\infty$ (i.e., $\text{Kn}\to\infty$), it is necessary that $\partial u_{\tau,\text{gas}}/\partial n\to 0$ in order to keep a finite difference $u_{\tau,\text{gas}}-u_{\tau,\text{wall}}$.

One interesting result of the model, relevant for design purposes, is the share of W_f between channel, stripper (sealing gap with $r>R_{\text{in}}$) and radial sealing ($r<R_{\text{in}}$) regions (see Figs. 1 and 2). Figure 9 shows these contributions to W_f for varying p_{out} (plotted here on a linear scale, in order to em-

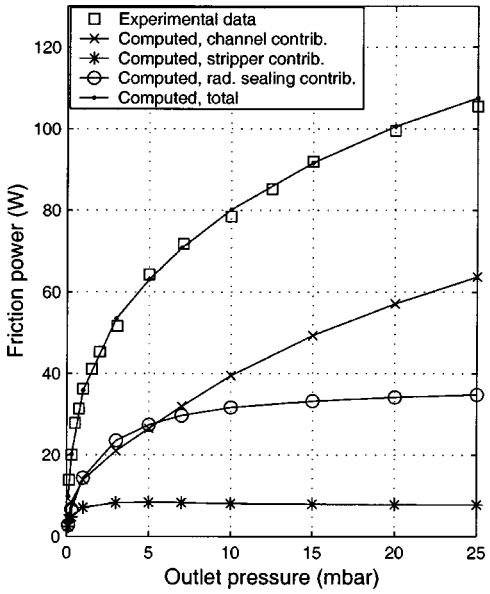

FIG. 9. Slip-flow model computed contributions to the friction power from different parts of the pump.

phasize the behavior at high pressure). We can see that most power is dissipated in the channel and in the radial sealing region. These two parts of the pump contribute to dissipate mechanical power, with a share of about 50% at low pressure, but with an increasing channel contribution at high pressure. The stripper contribution is small, owing to its small surface area, and saturates to a constant value quite early. Also the radial sealing contribution, like the stripper one, reaches an asymptotic value at high pressure, corresponding to laminar Couette flow in the gap; its variation at low pressure is due to the (transition) effect of the slip-flow boundary conditions. The channel contribution, which, like the radial sealing, exhibits the transition behavior at low pressure, maintains a positive slope even in viscous flow conditions ($p>10$ mbar, $\mathrm{Kn}<10^{-2}$, $\mathrm{Re}_h>800$).

This positive slope is found in the measured data and is maintained almost constant even at pressures higher than those presented in this work (up to 100 mbar). Cerruti *et al.* already noticed this behavior at high pressure,[5] but their one-dimensional model was not able to reproduce it, reaching, on the contrary, an asymptotic value. They attributed this disagreement to the possible onset of the instability of laminar flow (like Taylor vortices) or possibly turbulence.

Here we analyze the velocity profiles, in order to justify that positive slope, in the framework of the present NS laminar model. In Figs. 10, 11, 12 the contours of constant tangential velocity component $u_\vartheta(r,z,\vartheta=conts)$, are drawn on the restriction of section 1 to the channel (see Fig. 1 for reference), for $p_{\mathrm{out}}=1$, 10, 25 mbar, respectively. The closed islands on the contour plots represent the negative values of u_ϑ (Poiseuille backflow). These results are in qualitative agreement with the numerical results for shrouded rotor-stator systems by Randiamampianina *et al.*,[8] although the comparison is not exactly possible, since our problem is compressible and three-dimensional, with a tangential (along

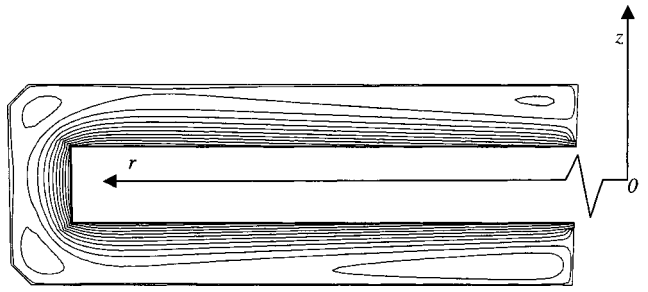

FIG. 10. Slip-flow model computed contours of constant $u_\vartheta(r,z,\theta=const)$ on section 1, $p_{\mathrm{out}}=1$ mbar.

ϑ) pressure gradient in the channel, while their problem is an incompressible, two-dimensional, pure Couette flow. Besides the shape of our channel is different from theirs.

Figure 10 refers to a situation characterized by $\mathrm{Re}_\phi \approx 10^3$: it shows the u_ϑ velocity contour pattern dominated by diffusive effects, with backflow regions close to the corners of the channel. Increasing the pressure, the flow pattern changes, owing to an increasing effects of radial convection. The centrifugal forces create a recirculating flow field in the channel: the gas flows radially outward close to the disc surface, and radially inward close to the stator walls (see Fig. 13, referred to $p_{\mathrm{out}}=25$ mbar). This radial velocity can be as high as 45 m/s for $p_{\mathrm{out}}=25$ mbar (about 13% of the maximum disc speed), and transports by convection u_ϑ. The result is the modification of the contour pattern for u_ϑ: the two backflow islands at the outer corners (high r) disappear, replaced by a small island at the tip of the disc. The contours of constant u_ϑ are stretched in radial direction close to the disc surface and the velocity gradient $\partial u_\vartheta/\partial z$ at the disc surfaces

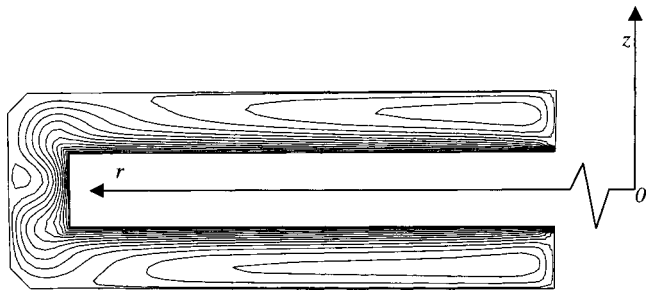

FIG. 11. Slip-flow model computed contours of constant $u_\vartheta(r,z,\theta=const)$ on section 1, $p_{\mathrm{out}}=10$ mbar.

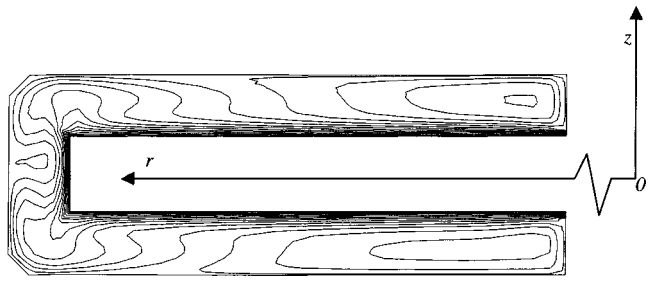

FIG. 12. Slip-flow model computed contours of constant $u_\vartheta(r,z,\theta=const)$ on section 1, $p_{\mathrm{out}}=25$ mbar.

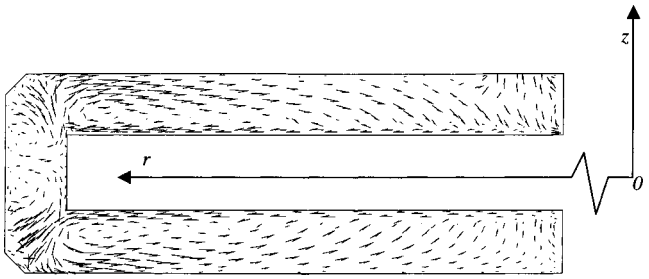

FIG. 13. Slip-flow model computed velocity vectors projected on section 1, $p_{out}=25$ mbar.

increases. For $p_{out}=25$ mbar ($\mathrm{Re}_\phi \approx 4.4\cdot 10^4$), two separate boundary layers (one at the stator, one at the rotor) seem to be going to develop at high r.

The increase of $\partial u_\vartheta/\partial z$ with the pressure justifies the increase of the channel contribution to W_f with p_{out}, in the framework of our laminar NS model.

The issue of laminar stability of the flow at high pressure, related to the oscillation detected for $p_{out}>25$ mbar, is still open, as this work does not answer the question of what actually happens in the Gaede pump in that limit. However, the extension of the simulation at even higher pressure than considered here is not very interesting from the design point of view, because the pump would not work efficiently for pressures much larger than that corresponding to the knee of the K vs p_{out} characteristics [about 10 mbar in this case, see Fig. 8(a)], where K drops dramatically. Sometimes the pumps are misused in the application, so that the interest in the possible unstable or turbulent flow in Gaede pumps is not only theoretical but even practical. This issue will possibly be the subject of a future work.

VI. CONCLUSIONS AND PERSPECTIVES

A transition model of the Gaede pump based on laminar NS equations with viscous slip and thermal jump boundary conditions was developed. It was solved in a pressure range covering three decades of Knudsen number, from viscous laminar ($\mathrm{Kn}\approx 10^{-3}$) to transition to molecular flow conditions ($\mathrm{Kn}\approx 1$), and covering the whole design operating pressure range of an experimental pump.

The validation against experimental data was carried out in terms of two engineering global quantities, compression ratio and friction power, showing a very good level of accuracy in the whole pressure range. The residual maximum error of about $+10\%$ for compression ratio and about $\pm 8\%$ for power (due to the uncertainty on the momentum accommodation coefficient) is small enough for design purposes, for which 10% precision is considered acceptable.

The model has a predictive nature, since the only parameters to be set are the properties of the gas and the momentum accommodation coefficient. Although the value of the latter is not known with precision, the variation on engineering parameters introduced by its maximum uncertainty is comparable with the uncertainty on the measured data. Hence the model can be used as a design tool to predict the performances and power dissipation of any geometrically different, possibly new, Gaede pump.

Instabilities and possibly turbulence effects can affect the behavior of the model at very high pressure, but this issue has not been developed here and could be the subject of future work, in case there is a demand from the designers in that direction.

The closer next step in the study of molecular drag pumps is going to consider heat exchange phenomena, in order to predict the rotor temperature in transition conditions, which is a critical design parameter in modern hybrid turbomolecular pumps.

ACKNOWLEDGMENT

The authors would like to thank Dr. John Helmer for reading the manuscript and giving useful suggestions for the interpretation of the numerical results.

APPENDIX A: SENSITIVITY TO THE ACCOMMODATION COEFFICIENTS

Since we did not know the exact value of the accommodation coefficients that, inserted in the Fluent built-in formulation [Eq. (7)], reproduce the correct values of σ_P and ς_T for nitrogen molecules on aluminum contaminated surfaces, we checked the sensitivity of the model to the variation of α_t and α_n. We considered an uncertainty interval for both α_t and α_n equal to (0.8, 1), including the maximum uncertainty interval found in the literature for nitrogen gas. We chose the case $p_{out}=1$ mbar, corresponding to a Knudsen number $\mathrm{Kn}\approx 10^{-1}$, and we checked the relative variation of K and W_f, after a variation of α_t and α_n of about $\pm 10\%$ with respect to a reference case $\alpha_t=\alpha_n=0.91$.

The results of this sensitivity study are listed in Table III. In the first part of the Table we kept α_n constant (=0.91) and varied α_t, between 0.8 and 1. The sensitivity of K is negligible (less than 0.5%). The sensitivity of W_f is on the contrary remarkable: about -8% for $\alpha_t=0.8$ and about 6% for $\alpha_t=1$. In the second part of Table III we kept α_t constant (=0.91) and varied α_n, between 0.8 and 1. The sensitivity of both K and W_f are less than 0.1%.

Since the precision required for the design of a pump is about 10%, we may conclude that, for design purposes, the only important parameter in our present case is the tangential momentum accommodation coefficient α_t. Besides only W_f is remarkably affected by the variation of this parameter with a non-negligible sensitivity. If we consider that the accuracy in the indirect measurement of W_f is about $\pm 5\%$, the uncertainty of the accommodation coefficient has, however, only a small effect for design purposes.

APPENDIX B: ONE-DIMENSIONAL COUETTE FLOW WITH SLIP-FLOW BOUNDARY CONDITIONS

We consider here the one-dimensional (1D) Couette flow problem,[15] solving it with viscous-slip boundary conditions, in order to show some of its features, relevant for the interpretation of the results of the three-dimensional (3D) work.

We consider two infinite parallel plates, a stationary and a moving one, and we want to calculate the y profile (in the direction transverse to the plates) of the x-component (along the plates) of the gas velocity, $u(y)$. Let h be the distance of the moving plate from the stationary one (placed at $y=0$) and V its velocity, directed along the x-axis. Since there are no pressure gradients, the NS equations with viscous slip boundary conditions reduce to:

$$\begin{cases} \mu \dfrac{d^2u}{dy^2} = 0, \\ u(0) = \sigma_P \lambda \left.\dfrac{du}{dy}\right|_{y=0}, \\ u(h) - V = -\sigma_P \lambda \left.\dfrac{du}{dy}\right|_{y=h}. \end{cases} \tag{B1}$$

The solution of the problem is

$$u(y) = A + By, \text{ with } \quad A = \frac{\sigma_P Kn}{1 + 2\sigma_P \mathrm{Kn}} V, \quad \text{and} \tag{B2}$$

$$B = \frac{1}{1 + 2\sigma_P \mathrm{Kn}} \frac{V}{h}. \tag{B2}$$

The solution shows a linear velocity profile, with slope B, decreasing with increasing Knudsen number ($\mathrm{Kn} = \lambda / h$).

Let us consider two interesting properties of this profile. The average velocity of the Couette flow is given by: $\bar{u} = 1/h \int_0^h u(y)dy = V/2$. It is independent of the Knudsen number.

The shear stress of the Couette flow is given by: $\tau_{xy} = \mu(du/dy) = [\mu/(1+2\sigma_P \mathrm{Kn})](V/h)$. It is independent of y; it shows a dependence on Kn, and $\tau_{xy} \to 0$ for $\mathrm{Kn} \to \infty$.

In the framework of the NS formulation with slip boundary conditions, we can conclude that one-dimensional Couette flow throughput does not change in the viscous-to-molecular transition, while the shear stress is remarkably affected by the Knudsen number in the transitional regime. Boulon *et al.*,[16] carried out a DSMC (direct simulation Monte Carlo) simulation of Couette flow between two parallel plates, in transition flow regime, for $10^{-2} < \mathrm{Kn} < 10^2$. They showed a linear velocity profile with the slip at the walls, matching the present 1D analysis, in molecular flow regime. Their results strangely move away from NS approaching the viscous regime, for $\mathrm{Kn} \to 10^{-2}$, producing a nonlinear velocity profile and a Couette pumping speed (or throughput) with a maximum in the transition regime. The difference showed by DSMC simulation, between Couette throughput in molecular and in viscous regime, is small (about 15% for 250 m/s wall velocity), and does not compromise our justification of the fact that K is scarcely affected by slip flow boundary conditions.

[1] S. Giors and F. Subba, J. Vac. Sci. Technol. A **22**, 1828 (2004).
[2] S. Chapman and T. G. Cowling, *The Mathematical Theory of Non-uniform Gases*, 3rd ed. (Cambridge University Press, Cambridge, 1970), Chap. 7, p. 110.
[3] M. N. Kogan, *Rarefied Gas Dynamics* (Plenum, New York, 1969).
[4] A. Beskok and G. E. Karniadakis, J. Thermophys. Heat Transfer **8**, 647 (1994).
[5] R. Cerruti, M. Spagnol, and J. C. Helmer, J. Vac. Sci. Technol. A **17**, 3096 (1999).
[6] J. C. Helmer and G. Levi, J. Vac. Sci. Technol. A **13**, 2592 (1995).
[7] J. W. Daily and R. E. Nece, J. Basic Eng. **82**, 217 (1960).
[8] A. Randriamampianina, L. Elena, J. P. Fontaine, and R. Schiestel, Phys. Fluids **9**, 1696 (1997).
[9] F. Sharipov, Eur. J. Mech. B/Fluids **22**, 133 (2003).
[10] J. C. Maxwell, Philos. Trans. R. Soc. London **170**, 169 (1879).
[11] C. Cercignani and M. Lampis, Transp. Theory Stat. Phys. **1**, 101 (1971).
[12] O. V. Sazhin, S. F. Borisov, and F. Sharipov, J. Vac. Sci. Technol. A **19**, 2499 (2001).
[13] J. M. Lafferty, *Foundations of Vacuum Science and Technology* (Wiley, New York, 1998), Chap. 1, p. 50.
[14] FLUENT 6.1 User's Guide (Fluent Inc., Lebanon, Pennsylvania, 2003)
[15] F. M. White, *Viscous Fluid Flow*, 2nd ed. (McGraw-Hill, Singapore, 1991), Chap. 3, p. 106.
[16] O. Boulon, R. Mathes, and J-P. Thibault, J. Vac. Sci. Technol. A **17**, 2080 (1999).